Power Grid Electromigration Checking Using Physics-Based Models

Sandeep Chatterjee, *Student Member, IEEE*, Valeriy Sukharev, and Farid N. Najm, *Fellow, IEEE*

***Abstract*—Due to technology scaling, electromigration (EM) signoff has become increasingly difficult, mainly due to the use of inaccurate methods for EM assessment, such as the empirical Black's model. In this paper, we present a novel finite-difference-based approach for power grid EM checking using physics-based models, that can account for process, voltage, and temperature variations across the die. Our main contribution is to extend existing physical models for EM in metal branches to track EM degradation in multibranch interconnect trees. The extended model is represented as a homogeneous linear time invariant system. We also detect early failures and account for their impact on grid lifetime. We speed up our implementation by proposing a macromodeling-based filtering scheme and a predictor-based approach. Our results, for a number of IBM power grid benchmarks, confirm that Black's model is overly inaccurate. The lifetimes found using our physics-based approach are on average 2.75× longer than those based on a (calibrated) Black's model, as extended to handle mesh power grids. With a maximum runtime of 2.3 h among all the IBM benchmarks, our method appears to be suitable for very large scale integration circuits.**

***Index Terms*—Electromigration (EM), hydrostatic stress, linear time invariant (LTI) systems, macromodeling, power grid, reliability, verification.**

I. Introduction

AS A RESULT of continued scaling of integrated circuits technology, electromigration (EM) has become a major reliability concern for the design of on-die power grids in large integrated circuits [1]. While signal and clock lines also suffer from EM degradation, these lines carry bidirectional current and so have longer lifetimes due to so-called *healing*. In contrast, power grid lines carry mostly unidirectional current with no benefit of healing and thus are more susceptible to EM failure. Hence, our focus on EM in power grids.

Today, it is becoming harder to sign off on chip designs using state of the art EM checking tools, as there is very little margin left between the predicted EM stress and that allowed by EM design rules [2]. This loss of safety margin can be traced back to the inaccurate and oversimplified nature of EM models used by existing tools. Standard practice in the industry is to break up a grid into isolated metal branches, assess the reliability of each branch *separately* using Black's model [3] and then use the series model (earliest branch failure time) to determine the failure time for the whole grid. This approach is highly *inaccurate*, for at least three reasons. First, the fitting parameters obtained for Black's model under accelerated testing conditions are not valid at actual operating conditions, and this leads to significant errors in lifetime extrapolation [4], [5].

Second, Black's model ignores the material flow between branches. In today's mesh structured power grids, many branches within the same layer are connected as part of what is called an *interconnect tree* (defined later) and atomic flux can flow freely between the branches of an interconnect tree. As a result, if the individual branches happen to be short so that they are deemed immortal due to the Blech effect [6], then the tree would appear to be immortal, which is highly *optimistic* and can be entirely misleading for design. In fact, due to material flow across the tree, failures can and do happen even if the branches are short. On the other hand, because the assumption of no material flow between branches effectively means that the reliability of nearby metal lines are independent of each other, then the traditional approach can also be highly *pessimistic*, as we will see in this paper. Indeed, two identical connected lines that carry the same current density can in practice have quite different values of mean time to failures (MTFs) [7], so that connected lines can influence each other leading to different mean lifetimes.

Finally, the third problem lies with the series model assumption. A series model is the case where a power grid is deemed to have failed as soon as the first of its branches has failed, typically due to an open circuit. However, modern power grids use a mesh structure. As such, there are many paths for the current to flow from the C4 bumps to the underlying logic, a characteristic we refer to as *redundancy*. Mesh power grids are in fact closer to (but not quite) a parallel system. As such, it is highly pessimistic to assume that a single branch failure will always cause the whole grid to fail.

Thus, there is a need to reconsider the traditional approaches and develop efficient EM checking techniques that can accurately assess EM degradation in large power grids.

Over the last few years, many approaches have been proposed which overcome, to some extent, the aforementioned shortcomings. Chatterjee *et al.* [8] proposed the *mesh model* as an alternative to the series model. In the mesh model, a grid is deemed to have failed, not when the first line fails,

Manuscript received September 14, 2016; revised December 20, 2016; accepted January 26, 2017. Date of publication February 9, 2017; date of current version June 18, 2018. This work was supported in part by the Natural Sciences and Engineering Research Council of Canada, and in part by Mentor Graphics Corporation. This paper was recommended by Associate Editor Y. Cao.

S. Chatterjee and F. N. Najm are with the Electrical and Computer Engineering Department, University of Toronto, Toronto, ON M5S 3G4, Canada (e-mail: sandeep.chatterjee@mail.utoronto.ca; f.najm@utoronto.ca).

V. Sukharev is with Mentor Graphics Corporation, Freemont, CA 94538 USA (e-mail: valeriy_sukharev@mentor.com).

Color versions of one or more of the figures in this paper are available online at http://ieeexplore.ieee.org.

Digital Object Identifier 10.1109/TCAD.2017.2666723

but when enough lines have failed so that the voltage drop at some grid node(s) have exceeded some predefined threshold (which would cause errors in underlying logic). However, [8] still used Black's model to compute the reliability of individual branches, which as we saw before is inaccurate. Huang *et al.* [9] proposed an adaptation of Korhonen's physical EM model [10] for interconnect trees. Hau-Riege and Thompson [11] used Korhonen's model to develop a closed form solution for stress evolution at a junction (a point where multiple branches meet) by replacing its connected branches with semi-infinite limbs, which was later used by Li *et al.* [12] in their EM verification tool. Both works [9], [12] were later extended in [13], [14] respectively to account for temperature variation as well. However, the approach in [9] is slow, requiring up to 32 h to estimate the failure time of a 400 k node grid. In [12], since the connected branches are replaced by semi-infinite limbs, atomic flow across the whole tree is *not* accounted for. Thus, there is a need for a new EM checking approach that accurately models EM degradation using physics-based models, combined with a mesh model to account for redundancy, while being fast enough to be practically useful.

In this paper, we propose such a technique, which is based on a finite-difference-based physical EM checking approach that accounts for process, voltage, and temperature variations across the die. A preliminary version of this paper is available in [15]. We start with Korhonen's 1-D physical model [10], and augment it: 1) by introducing *boundary laws* at junctions to track the material flow and stress evolution in multibranch interconnect trees (for arbitrary complex geometries) and 2) by accounting for thermal stresses generated by nonuniform temperature distribution across the grid. We refer to this as the *extended Korhonen's Model*. For each tree, the extended model starts out as a system of partial differential equations (PDEs) coupled by boundary laws which we then discretize and scale to reduce it to a *homogeneous* linear time invariant (LTI) system, where each state represents the stress at a discretized point in the tree. We numerically solve this system to track the stress evolution over time and find the corresponding time of void nucleations, some of which might cause early failures (EFs) by disconnecting a via. As we will show later, the impact of EF on grid reliability is quite severe, yet existing EM tools do not account for these failures. We are not aware of any published full-chip EM checking approach that can handle EFs. In this paper, we detect EFs and update the state of the system accordingly. We use the mesh model [8] to determine grid failure.

The random nature of EM degradation, caused by process variation, is taken care of by using a Monte Carlo method, in which successive samples of the grid time to failure (TTF) are found, until the estimate of the overall MTF has converged. We improve our runtime by using a macromodeling-based filtering scheme that estimates up-front the *active set of trees* that are most-likely to impact the MTF assessment of the grid, a scheme which we will show has minimal impact on accuracy. We also propose a predictive scheme that allows for fast MTF estimation based on extrapolation of the solution (stress curve) obtained from a few time-points. Testing this approach on the IBM grid benchmarks [16], with the largest grid up to 720 k nodes, shows that the MTF estimated using our physics-based approach are on average 2.75× longer than those based on a (calibrated) Black's model. This justifies the claim that Black's model can be overly inaccurate for modern power grids and confirms the need for physical models. With a run-time of 2.3 h for the most difficult to solve grid and 26 min for the largest (720 k) grid, this approach appears to be promising for large VLSI circuits.

The remainder of this paper is organized as follows. In Section II, we present some relevant background material regarding EM, numerical methods for solving PDEs and statistical methods which we will use later in this paper. Section III develops the extended Korhonen's model and Section IV describes the LTI system formulation used for numerically solving the extended model. Section V summarizes the approach we use to determine the temperature distribution and Section VI describes our overall power grid analysis approach. Section VII outlines the implementation details and discusses the experimental results. Finally, Section VIII concludes this paper.

II. Background

A. Electromigration Basics

EM is the mass transport of metal atoms due to momentum transfer between electrons (driven by an electric field) and the atoms in a metal line. EM is highly dependent on the specific microstructure of a given line. As such, due to random manufacturing variations, the TTF due to EM is a random variable (RV). The process of EM degradation can be divided into two phases: 1) void nucleation and 2) void growth.

Under conditions of high current density, metal atoms are pushed in the direction of the electron flow, which is opposite to the direction of the applied electric field. The number of atoms moving across a cross section of a line per second per unit area is known as the *atomic flux*. If the in-flow of metal atoms is equal to the out-flow at every point on the line segment, then clearly no deformation or failure will occur. On the other hand, if the in-flow is not equal to the out-flow, atomic flux divergence (AFD) is said to occur. AFD is a necessary prerequisite for EM degradation and is typically observed in locations with some kind of barrier to atomic movement, such as at the end of a line, or due to a change in widths of connected branches or due to change in diffusivity around grain boundaries. Flux divergence at these locations generates points of high tensile and compressive stresses within the segment. The amount of compressive stress needed to cause a pile-up of metal atoms (a *hillock*) leading to a short circuit is very high in modern metal systems, hence failure due to a short circuit is not usually observed. However, the build up of tensile stress eventually leads to formation of a *void* when the stress reaches a predetermined critical threshold. This phase of EM degradation, when stress is increasing over time but no voids have yet nucleated, is called the *void nucleation* phase. In this phase, the resistance of a line remains roughly the same as that of a fresh (undamaged) line.

Once a void nucleates, the *void growth* phase begins. In some cases, depending on the geometry and the location of

the void, nucleation by itself may be enough to cause failure due to an open circuit (by disconnecting a via) [17]. These failures are typically referred to as EFs and are often observed in testing. In other cases, again depending on geometry, a line may continue to conduct current after void nucleation. With time, the void starts to grow in the direction of the electron flow and the line resistance increases toward some steady-state value. In testing of single isolated lines, failure is deemed to happen when the increase in resistance reaches 10%–20% of the initial resistance value.

B. Korhonen Model

Korhonen *et al.* [10] proposed a 1-D model to describe the *hydrostatic stress* σ arising under the influence of EM. Here, hydrostatic stress is the average of all normal components of the full stress tensor, i.e., $\sigma = (\sigma_{xx} + \sigma_{yy} + \sigma_{zz})/3$. Consider a uniform metal line embedded in a rigid dielectric. We are interested in the time-varying stress $\sigma(x, t)$ at location x from some reference point, and at time t. Korhonen's model starts with the following statement

$$\Delta C(x, t) \big/ C(x, t) = -\Delta\sigma(x, t) \big/ B \tag{1}$$

where B is the bulk modulus and C is the number of metal atoms per unit volume, called the concentration of atoms. In an ideal lattice with zero stress, $C = 1/\Omega$, where Ω is the atomic volume. Following Korhonen's formulation, σ is positive for tensile stress and negative for compressive stress, and can be obtained by solving the PDE

$$\frac{\partial\sigma}{\partial t} = \frac{B\Omega}{k_b T_m}\frac{\partial}{\partial x}\left\{D_a\left(\frac{\partial\sigma}{\partial x} - \frac{q^*\rho}{\Omega}j\right)\right\} \tag{2}$$

where j is the current density in the line, D_a is the coefficient of atomic diffusion, k_b is the Boltzmann's constant, T_m is the temperature in Kelvin, q^* is the absolute value of the effective charge of the conductor, and ρ is the resistivity of the conductor. The corresponding atomic flux J_a in the line can be written as [10], [18]

$$J_a = \frac{D_a C\Omega}{k_b T_m}\left(\frac{\partial\sigma}{\partial x} - \frac{q^*\rho}{\Omega}j\right). \tag{3}$$

Note that J_a can be positive or negative, depending on the reference direction chosen and the actual direction of the electric current. A void nucleates in the line once the stress exceeds a predefined threshold value $\sigma_{\text{th}} > 0$.

C. Diffusivity of Metal Lines

The atomic diffusion coefficient D_a is usually expressed using the Arrhenius law

$$D_a = D_0 e^{-Q/(k_b T_m)} \tag{4}$$

where D_0 is a constant and Q is the activation energy for vacancy formation and diffusion. The randomness in TTF due to EM is primarily accounted for by the corresponding randomness in D_a, which is lognormally distributed [19] with mean D_{avg}. Strictly speaking, D_a also depends on the stress value at a given point. However, it has been reported that the numerical results with stress dependent D_a are "not too different" from constant D_a [10]. Hence, as in many previous works [9], [12]–[14], we will assume that D_a is stress-independent.

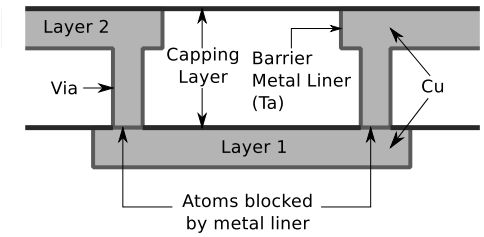

Fig. 1. Cross sectional schematic of Cu dual damascene interconnects.

D. Method of Lines

The method of lines (MoLs) is a special *finite-difference* technique for solving PDEs [20]. The basic idea of MoL is to discretize the PDE in *all but one* independent variable, so that we are left with a set of ordinary differential equations (ODEs) that approximate the PDE. We can then use well-established methods to numerically solve the ODE.

Discretizing the PDE along any variable requires us to approximate the partial derivatives. For a smooth function $f(\mathrm{x}_i, x_2, \ldots, x_n)$, the partial derivative with respect to x_i can be approximated using a *central difference formula* [20]

$$\frac{\partial f}{\partial \mathrm{x}_i}(x) \approx \frac{f(x + e_i\Delta x) - f(x - e_i\Delta x)}{2\Delta x} \tag{5}$$

$$\frac{\partial^2 f}{\partial \mathrm{x}_i^2}(x) \approx \frac{f(x + e_i\Delta x) + f(x - e_i\Delta x) - 2f(x)}{(\Delta x)^2} \tag{6}$$

where Δx is a small positive scalar increment and e_i is the ith unit vector (a vector that has 1 in position i and 0 elsewhere).

E. Limited Distributions

Let $\mathbf{Y}$ be an RV with cumulative distribution function (cdf) $F_Y(t)$ and let l and u be two scalars with $l < u$ and at least one of them finite. Then, RV $\mathbf{Y}'$ is called a *limited RV* between limits l and u, with $\mathbf{Y}$ being the underlying RV, if it has the following cdf [21]

$$F_{Y'}(t) = \begin{cases} 0, & t < l \\ F_Y(t), & l \le t < u \\ 1, & t \ge u. \end{cases} \tag{7}$$

III. Interconnect Tree EM Analysis

Modern power grids are made of copper (Cu) and are fabricated using a dual damascene process. In a dual-damascene process, the metal line and via are formed simultaneously using copper. A barrier metal liner (usually Tantalum) must completely surround all Cu interconnects to prevent the copper from diffusing into the surrounding dielectric. The cross section of a typical metal via structure in a Cu dual damascene process is as shown in Fig. 1. Every metal layer of the on-die power grid mostly consists of parallel stripes that are connected by vias to other metal layers. Note that due to the presence of the barrier metal liner around vias, Cu atoms from one layer cannot diffuse to another layer. On every layer, power and ground stripes are interspersed. As a result, the

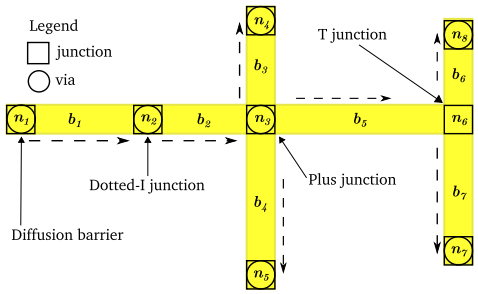

Fig. 2. Typical interconnect tree structure.

metal segments on every layer are mostly *trees*, i.e., they contain no loops or cycles. Thus, all previous work in this area assumes that the grid is made up of *interconnect trees*.

An interconnect tree is a continuously connected acyclic structure of straight metal lines within one layer of metalization such that atomic flux can flow freely within it. Fig. 2 shows a typical interconnect tree structure. Formally, an interconnect tree is a graph $\mathcal{T} = (\mathcal{N}, \mathcal{B})$ with no cycles, where $\mathcal{N}$ is a set of grid *junctions* and $\mathcal{B}$ is a set of resistive *branches*. A *branch* is defined to be a continuous straight metal line of uniform width. A *junction* is any point on the interconnect tree where a branch ends or where a via is located. Usually, but not always, current density around a junction is discontinuous. This discontinuity can be caused either by differences in the widths of connected branches, or by a change in the currents due to the presence of a via. We define the *degree* of a junction to be the number of branches connected to it. Note that a via does not contribute to the degree of a junction. In this paper, a junction with degree 1 will be referred to as a *diffusion barrier*, a junction with degree 2 will be referred to as a *dotted-I* junction, a junction with degree 3 will be referred to as a *T* junction and a junction with degree 4 will be referred to as a *plus* junction. We treat corners in a tree as *dotted-I* junctions. Junctions with degrees higher than 4 are rarely found in practice.

As in most recent works on EM, we assume that diffusivity D_a is the same throughout a branch. As a result, the AFD is higher at branch ends, i.e., junctions, as compared to branch interior. Thus, in our work, voids will nucleate only at junctions in a tree. This is a very mild assumption [12], [17] because it is much more common in the field to find voids at the end-points of branches. Also, it is worth noting that interconnect trees are *always* terminated by diffusion barriers and/or vias, hence the atoms cannot diffuse from one tree to another, and that different branches within a tree are allowed to have different widths.

A. Assigning Reference Directions

Before doing any analysis, we need to assign reference directions to all branches. This is necessary in order to consistently track the directions of branch currents and atomic flux.

An interconnect tree is equivalent to a graph, with grid junctions as vertices and branches as edges. Starting from any diffusion barrier, we traverse the whole interconnect tree using a *breadth-first search* on the graph. This creates predecessor–successor relationships between the junctions. The reference direction for each branch is then assigned from predecessor to successor. The branch current (and atomic flux) is positive if it flows in the reference direction, otherwise it is negative. Likewise, the reference point for distance is the predecessor junction, so that $x = 0$ is the predecessor and $x = L$ (line length) is the successor. In Fig. 2, if we choose to start from the leftmost diffusion barrier (labeled as n_1), then the reference directions for the branches would be as shown by the dashed arrows.

B. Initial Conditions

Initial conditions determine the stresses in the interconnect tree at $t = 0$, before the application of any electric current. For on chip interconnects, the metal lines are embedded in a rigid confinement. Because of the difference in the coefficients of thermal expansion of the metal (Cu) a_m and confinement (silicon) a_{si}, stress is generated as the metal cools down after deposition. This so called thermal stress can be expressed as [22]

$$\sigma_{T,k}(t) = B(a_m - a_{si})(T_{zs} - T_{m,k}(t)) \tag{8}$$

where $\sigma_{T,k}$ is the thermal stress, $T_{m,k}$ is the temperature of branch b_k, and T_{zs} is the stress free annealing temperature. In this paper, we assume that the initial stress $\sigma_k(x_k, 0)$ in branch b_k is equal to its thermal stress at $t = 0$, so that

$$\sigma_k(x_k, 0) = \sigma_{T,k}(0). \tag{9}$$

C. Extending Korhonen's Model to Trees

In order to find the level of EM degradation in an interconnect tree, we will extend Korhonen's model to account for the coupling between the tree branches. For better understanding, we illustrate our approach with a simple example. Consider a simple tree $\mathcal{T}_d = (\mathcal{N}, \mathcal{B})$, with $\mathcal{N} = \{n_1, n_2, n_3\}$ and $\mathcal{B} = \{b_1, b_2\}$, with reference directions as shown in Fig. 3. Branch b_k has dimensions $L_k \times w_k \times h_k$ (length $\times$ width $\times$ height), carries a current density j_k, has an atomic diffusivity of $D_{a,k}$ and temperature $T_{m,k}$, where k is 1 or 2 in this case. Note that $x_1 = L_1$ and $x_2 = 0$ denote the same point: the location of n_2. We are interested in the stress as a function of position and time, i.e., $\sigma_1(x_1, t)$ and $\sigma_2(x_2, t)$ for branches b_1 and b_2, respectively. Once σ_1 and σ_2 are known, we can easily determine the EM degradation in the branches.

Korhonen's model (2) gives the time rate of change of stress for a point *within* a branch, as follows:

$$\frac{\partial \sigma_k}{\partial t} = \frac{B\Omega D_{a,k}}{k_b T_{m,k}} \frac{\partial}{\partial x_k}\left(\frac{\partial \sigma_k}{\partial x_k} - \frac{q^* \rho}{\Omega} j_k\right), \quad x_k \in (0, L_k). \tag{10}$$

However, in order to solve the PDE for the whole tree, we need to also state the boundary conditions at all end-points of branches, i.e., at junctions. The boundary conditions describe the behavior of atomic flux at the junctions. For the example in Fig. 3, we will discuss the two cases of a diffusion barrier and a dotted-I junction.

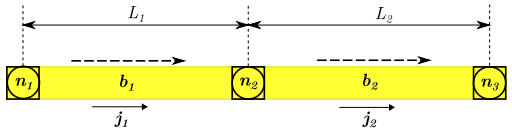

Fig. 3. Simple 3-terminal tree $\mathcal{T}_d$.

1) Diffusion Barrier: Junctions n_1 and n_3 are diffusion barriers, where the atomic flux is blocked. Considering the nucleation phase first, J_a is zero at the barrier so that from (3)

$$J_{a,1}(0,t)=0 \implies \frac{\partial \sigma_1(0,t)}{\partial x_1}=\frac{q^*\rho}{\Omega}j_1 \tag{11a}$$

$$J_{a,2}(L_2,t)=0 \implies \frac{\partial \sigma_2(L_2,t)}{\partial x_2}=\frac{q^*\rho}{\Omega}j_2. \tag{11b}$$

We next move to the void growth phase. For a void to nucleate at n_1 (n_3), we must have $j_1<0$ ($j_2>0$) so that the electron flow pushes the metal atoms away from n_1 (n_3). Exactly what happens around a void is somewhat complicated and cannot be fully captured in a 1-D model. The recent work in [22] provides an extension of the Korhonen 1-D model to describe behavior of stress around a void. From this, stress falls to zero at the void surface but remains at its original value a very short distance $\delta \approx 1$ nm from the void surface. We refer to δ as the *thickness of the void interface*. From [22], the stress gradients at junctions n_1 and n_3 throughout the void growth phase are

$$\frac{\partial \sigma_1(0,t)}{\partial x_1}=\frac{\sigma_1(0,t)}{\delta}, \quad \frac{\partial \sigma_2(L_2,t)}{\partial x_2}=-\frac{\sigma_2(L_2,t)}{\delta} \tag{12}$$

where $\sigma_1(0,t)=\sigma_2(L_2,t)=\sigma_{\text{th}}$ at the time of void nucleation.

2) Dotted-I Junction: The atomic flux interaction at dotted-I junction n_2 is the key to describing the coupling of stresses in branches b_1 and b_2. Considering the nucleation phase first, the stress is continuous across n_2, which is the same physical point of both b_1 and b_2, so that

$$\sigma_1(L_1,t)=\sigma_2(0,t) \tag{13}$$

and atomic flux can flow freely between b_1 and b_2 [11]. Because the material flow across an infinitesimal boundary at n_2 has to be continuous, we have

$$w_1h_1J_{a,1}(L_1,t)=w_2h_2J_{a,2}(0,t). \tag{14}$$

Next considering the void growth phase, once a void nucleates at n_2, it is shared by both branches b_1 and b_2. For our 1-D model, we make the reasonable assumption that the void covers the entire cross sectional area of the junction. As a result, there would be no flow of atomic flux between b_1 and b_2. Hence, during the *void growth* phase, we effectively treat n_2 as a diffusion barrier for both branches b_1 and b_2, so that

$$\frac{\partial \sigma_1(L_1,t)}{\partial x_1}=-\frac{\sigma_1(L_1,t)}{\delta}, \quad \frac{\partial \sigma_2(0,t)}{\partial x_2}=\frac{\sigma_2(0,t)}{\delta}. \tag{15}$$

As we will see later in Section IV, combining the boundary conditions obtained from (11)–(15) and the initial condition as stated in (9) with (10), we can formulate an LTI system that completely determines σ_1 and σ_2. We will next generalize the above schemes for capturing flux interactions at junctions, into a set of *laws* that forms the basis for our approach.

D. Boundary Laws for Junctions

Boundary laws govern the interaction of atomic flux at junctions. Consider a junction n_p, and let $\mathcal{B}_p$ be the set of branches connected to n_p. Let $t_{f,p}$ be the time of void nucleation for this junction. Then, the boundary laws (motivated mainly by the law of conservation of mass) can be stated as follows.

Law 1: For $t<t_{f,p}$, the number of metal atoms flowing into n_p per unit time is the same as the number of metal atoms flowing out from it

$$\sum_{b_k\in\mathcal{B}_{p,\text{in}}} w_kh_kJ_{a,k}=\sum_{b_k\in\mathcal{B}_{p,\text{out}}} w_kh_kJ_{a,k} \tag{16}$$

where w_k (h_k) is the width (height) of the branch, $\mathcal{B}_{p,\text{in}}$ is the set of branches for which the reference direction is going into n_p, and $\mathcal{B}_{p,\text{out}}$ is the set of branches for which the reference direction is going out from n_p.

Law 2: For $t\geq t_{f,p}$, there is no flow of atomic flux between the connected branches $\mathcal{B}_p$. The stress gradient at the junction, generalizing from (12) and (15), is

$$\frac{\partial \sigma_{k,p}}{\partial x_k}=\pm\frac{\sigma_{k,p}}{\delta} \tag{17}$$

where $\sigma_{k,p}$ is the value of stress at end-point n_p of branch b_k. The sign is positive for $b_k\in\mathcal{B}_{p,\text{out}}$ and negative for $b_k\in\mathcal{B}_{p,\text{in}}$.

Law 3: Until a void nucleates at n_p, the stress values in any two branches where they meet at n_p are equal.

E. Handling Void Growth and Early Failures

Once the stress at any point in the tree reaches σ_{th}, a void nucleates at that point. As noted before, in our EM model, void nucleation occurs only at junctions and not within the branches. We assume that once a void nucleates at a junction, it is shared by all the branches connected to that junction. Tracking void growth is useful in order to determine the change in branch resistances and the corresponding current densities. In addition, we also check for EFs depending on the location of the void.

Recent work [22] shows that the initial void growth rate is very high. Hence, as a conservative approximation, we assume that once a void nucleates at any junction n_p, the void lengths for all branches b_k connected to n_p reach their steady state values in a very short period of time. As a result, the line resistance rises immediately to its steady state value for all connected branches. The steady state void volume for branch b_k is

$$\mathcal{V}_{k,\text{sat}}=L_kw_kh_k\left(\frac{\sigma_{T,k}}{B}+\frac{q^*\rho|j_k|L_k}{2B\Omega}\right). \tag{18}$$

Based on this, we iteratively find j_k and $\mathcal{V}_{k,\text{sat}}$ using a modified Richardson iteration. We ignore void healing and void migration.

Depending on its location and size, a void might lead to an EF. Specifically, if a large enough void forms *below a via*, it might in some cases cause an open circuit failure by disconnecting the via. This happens because the capping layer is *not conductive*; hence if the void covers the entire cross section of a via, there is no conductive path left between the via and the tree below and the current in the via completely

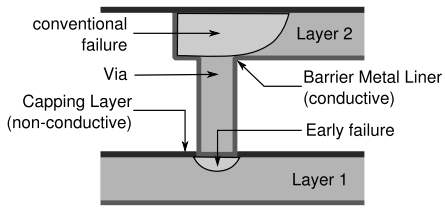

Fig. 4. EFs and conventional failures.

falls to 0, as shown in Fig. 4. On the other hand, voids that form above the via generally happen at the top of the line away from the via, and so take a long time to completely fill the cross section, and even then do not translate to an open circuit because the current can continue to flow through the metal liner. Removal of a via, as it happens during the EFs, can have a significant impact on grid reliability and thus should be accounted for. In our model, once we have determined the steady state void volume using (18), we check 1) if the void is located below a via (this is determined based on geometry of the grid) and 2) if the void is large enough to disconnect the via. If both conditions are met, this void leads to an EF, so that we remove the via from the power grid and update the voltage drops and current density values.

IV. Solving the Extended Model

In this section, we will describe our approach for solving the extended Korhonen's model for trees. First, for points within a branch, we will use the MoLs to convert the PDEs into a set of ODEs. Then, using the laws proposed in Section III-D, we will derive the boundary conditions at the junctions. Finally, we merge the two and state the LTI system formulation that describes the stress evolution for a given tree.

A. Scaling Korhonen's Model

Korhonen's model (2) is often scaled by introducing dimensionless variants of stress, length, and time [18]. This leads to stable PDEs that are easier to solve numerically. We define the following scaling factors for any branch $b_k \in \mathcal{B}$:

$$\tau \triangleq \frac{B\Omega}{k_b T_m^\star}\frac{D_a^\star t}{L_c^2}, \quad \eta_k \triangleq \frac{\Omega\sigma_k}{k_b T_m^\star}, \quad \xi_k \triangleq \frac{x_k}{L_k} \tag{19}$$

where $D_a^\star$ is the atomic diffusivity at some chosen nominal temperature $T_m^\star$, L_c is some chosen characteristic length and $0 \le x_k \le L_k$. The new variables τ, η, and ξ are referred to as reduced time, stress, and distance, respectively. Using (19) in (2) and applying the chain-rule, we get

$$\frac{\partial \eta_k}{\partial \tau} = \theta_k \frac{\partial}{\partial \xi_k}\left(\frac{\partial \eta_k}{\partial \xi_k} - \alpha_k\right) \tag{20}$$

where $\theta_k = (L_c^2 D_{a,k} T_m^\star / L_k^2 D_a^\star T_{m,k})$, $\alpha_k = (q^* \rho j_k L_k / k_b T_m^\star)$, j_k is the current density, $T_{m,k}$ is the temperature, and $D_{a,k}$ is the diffusivity for b_k. Since, for any given branch, α_k is not a function of distance ξ_k, then $\partial\alpha_k/\partial\xi_k = 0$ and we get

$$\frac{\partial \eta_k}{\partial \tau} = \theta_k \frac{\partial^2 \eta_k}{\partial \xi_k^2}. \tag{21}$$

For any branch b_k, (21) constitutes the scaled PDE system to be solved. Also, the atomic flux in b_k can be restated in terms of reduced variables

$$J_{a,k} = \frac{D_{a,k} C T_m^\star}{L_k T_{m,k}}\left(\frac{\partial \eta_k}{\partial \xi_k} - \alpha_k\right). \tag{22}$$

B. Discretization for Tree Branch

We uniformly discretize branch b_k into N segments, where N is the same for all branches [because we have scaled all branch lengths to 1 as in (19)]. The reduced stress at each of the $N+1$ discrete spatial points $\{0, \ldots N\}$ is denoted by $\eta_{k,i}$ and the time rate of change of $\eta_{k,i}$ is [from (21)]

$$\frac{\partial \eta_{k,i}}{\partial \tau} = \theta_k \frac{\partial^2 \eta_{k,i}}{\partial \xi_k^2} \quad \text{for } i = 0, 1, \ldots, N. \tag{23}$$

Further, we approximate the partial derivatives with respect to ξ using central difference approximation, so that (23) leads to

$$\frac{\mathrm{d}\eta_{k,i}}{\mathrm{d}\tau} = \theta_k\left(\frac{\eta_{k,i+1} + \eta_{k,i-1} - 2\eta_{k,i}}{(\Delta\xi)^2}\right) \tag{24}$$

where $\Delta\xi = \Delta\xi_k = 1/N$, $\forall k$. The corresponding atomic flux $J_{a,k,i}$ at the ith point is

$$J_{a,k,i} = \frac{D_{a,k} C T_m^\star}{L_k T_{m,k}}\left(\frac{\eta_{k,i+1} - \eta_{k,i-1}}{2\Delta\xi} - \alpha_k\right). \tag{25}$$

Note that for each branch, the ODEs at junctions ($i = \{0, N\}$) require the values for $\eta_{k,-1}$ and $\eta_{k,N+1}$, which are *not* part of the ξ_k domain. The values at these *ghost points* are obtained by solving for the respective boundary condition(s), as we next explain.

In order to simplify the presentation going forward, we define the following for any two branches $b_i, b_k \in \mathcal{B}$:

$$\begin{aligned} r_{ik} &= L_i/L_k, \quad p_{ik} = D_{a,i} T_{m,k}/(D_{a,k} T_{m,i}) \\ w_{ik} &= w_i/w_k, \quad \gamma_{ik} = r_{ki} w_{ik} p_{ik}, \quad \Upsilon_k = \theta_k/(\Delta\xi)^2. \end{aligned} \tag{26}$$

C. Boundary Conditions at Diffusion Barrier

Consider a diffusion barrier n_p connected to branch b_k. We have two cases, one where n_p is at the predecessor junction ($\xi_k = 0$, start of the branch) and one where it is at the successor junction ($\xi_k = 1$, branch end). We first obtain the boundary conditions for n_p at $\xi_k = 0$. Let τ_f be the time of void nucleation at this barrier. Then, the corresponding boundary condition is [using (16) and (17)]

$$\frac{\partial \eta_{k,0}}{\partial \xi_k} = \begin{cases} \alpha_k & \tau < \tau_f \\ \eta_{k,0}(L_k/\delta) & \tau \ge \tau_f \end{cases} \tag{27}$$

where $\eta_{k,0}$ corresponds to $\sigma_{k,p}$ in (17), with $\eta_{k,0} = \eta_{\text{th}} = (\Omega\sigma_{\text{th}})/(k_b T_m^\star)$ at $\tau = \tau_f$.

Using the central difference approximation, we get

$$\eta_{k,-1} = \begin{cases} \eta_{k,1} - 2\Delta\xi\alpha_k & \tau < \tau_f \\ \eta_{k,1} - 2\Delta\xi\eta_{k,0}(L_k/\delta) & \tau \ge \tau_f. \end{cases} \tag{28}$$

Similarly, for a diffusion barrier at $\xi_k = 1$, we get

$$\eta_{k,N+1} = \begin{cases} \eta_{k,N-1} + 2\Delta\xi\alpha_k & \tau < \tau_f \\ \eta_{k,N-1} - 2\Delta\xi\eta_{k,N}(L_k/\delta) & \tau \ge \tau_f. \end{cases} \tag{29}$$

D. Boundary Conditions at Dotted-I Junction

Consider a dotted-I junction n_p. Without loss of generality, we will assume that n_p is at the end of branch 1 and at the beginning of branch 2. To solve the ODE at n_p, we need the value of at least one of the ghost points ($\eta_{1,N+1}$ or $\eta_{2,-1}$). Let τ_f be the time of void nucleation at this junction. Then, using (16), we get ($h_1 = h_2$ within a metal layer)

$$w_1 J_{a,1,N} - w_2 J_{a,2,0} = 0 \quad \text{for } \tau < \tau_f. \tag{30}$$

Also, from law 3, $\eta_{1,N} = \eta_{2,0}$ when $\tau < \tau_f$. Hence, the time rate of change of stress should also be the same, so that using (21)

$$\frac{\partial \eta_{1,N}}{\partial \tau} = \frac{\partial \eta_{2,0}}{\partial \tau} \implies \frac{\partial^2 \eta_{1,N}}{\partial \xi_1^2} = \frac{\theta_2}{\theta_1} \frac{\partial^2 \eta_{2,0}}{\partial \xi_2^2} \text{ for } \tau < \tau_f. \tag{31}$$

Substituting the value of J from (25) to (30) and applying the central difference formula in (31), we can obtain the value of ghost points. Due to lack of space, we omit the full derivation and only present the final value of $\eta_{1,N+1}$

$$\eta_{1,N+1} = \eta_{1,N-1} + (r_{12}u_1 + w_{21}u_2)/(r_{12} + w_{21}) \tag{32}$$

where $u_2 = 2(r_{12}^2 p_{21}\eta_{2,1} - \eta_{1,N-1} + (1 - r_{12}^2 p_{21})\eta_{1,N})$ and $u_1 = 2\Delta\xi(\alpha_1 - \gamma_{21}\alpha_2)$.

Using law 2, n_p is treated as a diffusion barrier for both branches during the void growth phase. Thus, for $\tau \geq \tau_f$

$$\eta_{1,N+1} = \eta_{1,N-1} - 2\Delta\xi\eta_{1,N}(L_1/\delta) \tag{33a}$$

$$\eta_{2,-1} = \eta_{2,1} - 2\Delta\xi\eta_{2,0}(L_2/\delta). \tag{33b}$$

The corresponding boundary conditions for T and *plus* junctions can be obtained by following the same procedure as done for the dotted-I junction.

E. LTI System Formulation

Consider a tree $\mathcal{T} = \{\mathcal{N}, \mathcal{B}\}$ with $|\mathcal{N}|$ junctions and $|\mathcal{B}|$ branches, with each branch discretized into N segments. Then, there would be a total of $q+1$ discretized points, where $q = N|\mathcal{B}|$. Note that two points are said to be *adjacent* to each other if they are physically next to each other in the tree. Let each discretized point be given a unique index $i \in \{0, 1, 2, \ldots q\}$ and let x_i represent the reduced stress at ith discretized point in the tree. Then, the ODEs (24) for branches $b_k \in \mathcal{B}$, combined with initial and boundary conditions can be represented as a first-order ODE system consisting of $q+1$ equations and $q+1$ states, namely x_i. The outputs of the system will be the states at the junctions. Let $\hat{\mathbf{A}} = [\hat{a}_{i,k}] \in \mathbb{R}^{(q+1)\times(q+1)}$ be the system matrix and $\hat{\mathbf{B}} = [\hat{b}_{i,k}] \in \mathbb{R}^{(q+1)\times|\mathcal{N}|}$ be the input matrix for the ODE system. Each state x_i, depending on its location and the *phase* of EM degradation, "contributes" some nonzero entries to the *ith* row of $\hat{\mathbf{A}}$ and $\hat{\mathbf{B}}$, which we will refer to as a *state stamp*. Due to space constraints, we will only present the state stamps for $\hat{\mathbf{A}}$ before any void nucleation occurs.

1) Branch Interior: Consider state x_i for a discretized point within branch b_k. Let i_1 and i_2 be the indices for the two adjacent points. Then, the nonzero entries of the ith row are

$$\hat{a}_{i,i} = -2\Upsilon_k, \quad \hat{a}_{i,i_1} = \hat{a}_{i,i_2} = \Upsilon_k. \tag{34}$$

2) Diffusion Barrier: Consider state x_i for a diffusion barrier at the beginning or the end of branch b_k. Let the index of the (only) adjacent point be i_1. Then, we have

$$\hat{a}_{i,i} = -2\Upsilon_k, \quad \hat{a}_{i,i_1} = 2\Upsilon_k. \tag{35}$$

3) Dotted-I Junction: Without loss of generality, we will assume that the dotted-I junction with state x_i is at the end of branch 1 and at the beginning of branch 2. Further, the dotted-I junction is adjacent to point i_1 from branch 1 and point i_2 from branch 2. Then the corresponding nonzero entries will be

$$\begin{aligned} \hat{a}_{i,i} &= -2\varrho_{12}\Upsilon_1(\gamma_{11} + \gamma_{21}), \\ \hat{a}_{i,i_k} &= 2\varrho_{12}\Upsilon_1\gamma_{k1}, \quad k = 1, 2 \end{aligned} \tag{36}$$

where $\varrho_{12} = r_{12}/(r_{12} + w_{21})$.

4) T Junction: Similar to the dotted-I junction, we will assume that the T junction with state x_i is at the end of branch 1 and at the beginning of branches 2 and 3. The indices of the adjacent points in branches 1, 2, and 3 are i_1, i_2, and i_3, respectively. Then the nonzero entries of the ith row are

$$\begin{aligned} \hat{a}_{i,i} &= -2\varrho_{13}\Upsilon_1(\gamma_{11} + \gamma_{21} + \gamma_{31}), \\ \hat{a}_{i,i_k} &= 2\varrho_{13}\Upsilon_1\gamma_{k1}, \quad k = 1, 2, 3 \end{aligned} \tag{37}$$

where $\varrho_{13} = (r_{12}r_{13})/(r_{12}r_{13} + r_{13}w_{21} + r_{12}w_{31})$.

5) Plus Junction: For a plus junction with state x_i, assuming that it is at the end of branch 1 and at the beginning of branches 2–4; the nonzero entries are

$$\begin{aligned} \hat{a}_{i,i} &= -2\varrho_{14}\Upsilon_1(\gamma_{11} + \gamma_{21} + \gamma_{31} + \gamma_{41}), \\ \hat{a}_{i,i_k} &= 2\varrho_{14}\Upsilon_1\gamma_{k1}, \quad k = 1, 2, 3, 4 \end{aligned} \tag{38}$$

where i_1, i_2 i_3, and i_4 are the points adjacent to the ith point in branches 1–4, respectively, and $\varrho_{14} = (r_{12}r_{13}r_{14})/(r_{12}r_{13}r_{14} + r_{13}r_{14}w_{21} + r_{12}r_{14}w_{31} + r_{12}r_{13}w_{41})$.

From (34) to (38), it is clear that $\hat{\mathbf{A}}$ is diagonally dominant with all row sums being 0 and all its diagonal entries are negative. Hence, by Gershgorin circle theorem [23], all eigenvalues of $\hat{\mathbf{A}}$ must lie in the left half of the complex plane. Also, by construction, we have $\hat{\mathbf{A}}z = 0$ for $z = [1 \quad 1 \quad \ldots \quad 1]^T$ or a multiple thereof. Thus, $\hat{\mathbf{A}}$ has at least one 0 eigenvalue and is a singular matrix. This happens because an interconnect tree is a closed system, i.e., there is no exchange of atoms with the other trees. This creates a dependency among the x_i variables, which we will now show.

By *conservation of mass*, the number of atoms in the tree will remain the same at all times. From (1), we can write

$$C(x, t) = C_0 e^{-\sigma(x,t)/B} \tag{39}$$

where $C(x, t)$ is the concentration of atoms and C_0 is its equilibrium value in the absence of stress. Then, the total number of atoms $\mathcal{A}_{\text{tot}}$ in the tree at any time t can be written as (h, the height of the tree is same for all branches)

$$\begin{aligned} \mathcal{A}_{\text{tot}} &= C_0 h \sum_{b_k \in \mathcal{B}} w_k \int_0^{L_k} e^{-\sigma_k(x_k,t)/B}\, \mathrm{d}x_k \\ &\approx C_0 h \sum_{b_k \in \mathcal{B}} w_k \int_0^{L_k} (1 - \sigma_k(x_k, t)/B)\, \mathrm{d}x_k \\ &= \frac{C_0 h}{B} \left(B \sum_{b_k \in \mathcal{B}} w_k L_k - \sum_{b_k \in \mathcal{B}} w_k \int_0^{L_k} \sigma_k(x_k, t)\, \mathrm{d}x_k \right) \end{aligned} \tag{40}$$

where we used the approximation $e^x \approx 1 + x$ for $x \ll 1$ because $\sigma_k(x_k, t) \ll B$, $\forall t$. Clearly, only the stress values in the second summation term in (40) change with time; everything else remains constant. Therefore, the tensile/compressive stresses generated by the movement of atoms can only vary in a way that satisfies the conservation of mass. Define

$$\beta(\tau) \triangleq \sum_{b_k \in \mathcal{B}} w_k L_k \int_0^1 \eta_k(\xi_k, \tau) d\xi_k \tag{41}$$

which is the second summation term in (40) rewritten in terms of the reduced stress. Since the stress values for all points at $\tau = 0$ is known from initial conditions, $\beta(0) = \beta_0$ is always a known quantity. Then, in order to satisfy the conservation of mass, we must have $\beta(0) = \beta(\tau)\ \forall \tau$. Evaluating the integral in (41) using the trapezoidal rule, we can write

$$\beta_0 = \sum_{i=0}^{q} c_i \mathrm{x}_i(\tau) \tag{42}$$

where c_i are the coefficients as determined by the trapezoidal rule. This gives us a linear dependence between x_i so that one state can be eliminated. Without loss of generality, let x_0 be a nonoutput state to be eliminated. Define

$$\mathrm{x}(\tau) \triangleq \begin{bmatrix} \mathrm{x}_1(\tau) & \mathrm{x}_2(\tau) & \dots & \mathrm{x}_{q-1}(\tau) & \mathrm{x}_q(\tau) \end{bmatrix}^T \tag{43}$$

to be the state vector. Now, we can write

$$\mathrm{x}_0(\tau) = -c^T \mathrm{x}(\tau) + \beta_0 / c_0 \tag{44}$$

where $c = c_0^{-1}[\, c_1\, c_2\, \dots\, c_q\,]^T \in \mathbb{R}^q$. Using (44) and the previous ODE formulation, we can eliminate x_0 from the ODE equations (thereby removing the eigenvalue at 0) so that the stress evolution in a tree can be represented by an LTI system with q ODE equations with q independent states:

$$\dot{\mathrm{x}}(\tau) = \mathbf{A}\mathrm{x}(\tau) + \mathbf{B}u \tag{45a}$$
$$\mathrm{y}(\tau) = \mathbf{L}\mathrm{x}(\tau) \tag{45b}$$
$$\mathrm{x}(0) = \begin{bmatrix} \eta_{T,1}(0) & \eta_{T,2}(0) & \dots & \eta_{T,q}(0) \end{bmatrix} \tag{45c}$$

where $\eta_{T,i}(0)$ is the reduced thermal stress at $t = 0$ at the ith discretized point, $u \in \mathbb{R}^{|\mathcal{N}|}$ is the input vector which depends on the branch current densities, $\mathbf{A} \in \mathbb{R}^{q \times q}$ is the system matrix and $\mathbf{B} \in \mathbb{R}^{q \times |\mathcal{N}|}$ is the input matrix such that

$$\mathbf{A} = -\hat{a}_q c^T + \hat{\mathbf{A}}_q \tag{46a}$$
$$\mathbf{B} = \hat{\mathbf{B}}_q + (\beta_0/c_0)\hat{a}_q \bar{u}^T,\ \bar{u} \in \mathbb{R}^{|\mathcal{N}|} \text{ and } \bar{u}^T \cdot u = 1 \tag{46b}$$

with $\hat{a}_q = [\hat{a}_{i,k}]$ for $1 \le i \le q, k = 0$, $\hat{\mathbf{A}}_q = [\hat{a}_{i,k}]$ for $1 \le i, k \le q$ and $\hat{\mathbf{B}}_q = [\hat{b}_{i,k}]$ for $1 \le i \le q, 0 \le k \le |\mathcal{N}| - 1$. The output $\mathrm{y}(\tau) \in \mathbb{R}^{|\mathcal{N}|}$ is the vector of stress values at the junctions and $\mathbf{L} \in \mathbb{R}^{|\mathcal{N}| \times q}$ is the output matrix.

Between any two void nucleations, $\mathbf{A}$, $\mathbf{B}$ and input u are constant. Hence, we can further simplify the LTI system representation by applying the following change of variables:

$$\hat{\mathrm{x}}(\tau) = \mathrm{x}(\tau) - \mathrm{x}_{ss} \tag{47}$$

where $\mathrm{x}_{ss} = -\mathbf{A}^{-1}\mathbf{B}u$ is the steady state stress of the tree for the given input u. Finally, we can rewrite (45) as

$$\dot{\hat{\mathrm{x}}}(\tau) = \mathbf{A}\hat{\mathrm{x}}(\tau) \tag{48a}$$

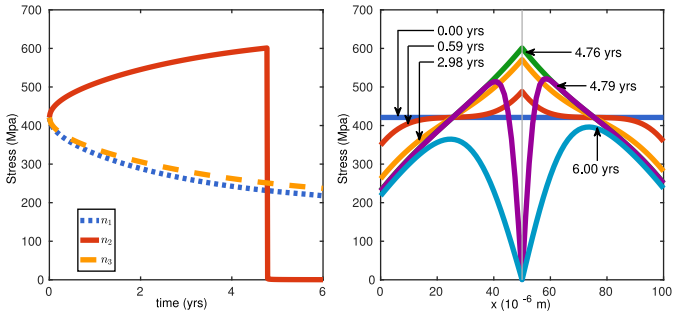

(a) (b)

Fig. 5. For $\mathcal{T}_d$, (a) evolution of stress at junctions with time and (b) stress profile with time. Here, $L_1 = L_2 = 50$ μm, and $j_1 = -j_2 = 6e9$ A/m^2.

$$\mathrm{y}(\tau) = \mathbf{L}(\hat{\mathrm{x}}(\tau) + \mathrm{x}_{ss}) \tag{48b}$$
$$\hat{\mathrm{x}}(0) = \mathrm{x}(0) - \mathrm{x}_{ss}. \tag{48c}$$

We solve this LTI system using *adaptive step Runge–Kutta* methods, and the solution for $\mathcal{T}_d$ of Fig. 3 is shown in Fig. 5.

F. Interconnect Tree Macromodeling

The full size (order) of the LTI system representation of a tree is $q = N|\mathcal{B}|$. As such, the resulting system may become very large for finer discretizations or for large trees. Thus, to reduce the computation time, we propose a model order reduction technique based on the *Arnoldi process* [23] that calculates the stress profile of a tree for any given time τ. We will use this technique later in Sections VI-B and VI-C for improving the performance of our power grid EM analysis.

Using (47) and (48), we can write

$$\mathrm{x}(\tau) = e^{\mathbf{A}\tau}\hat{\mathrm{x}}(0) + \mathrm{x}_{ss} \tag{49}$$

for which a direct analytical solution may be possible. But, calculating the matrix exponential at any given time point for the full order system is computationally expensive. However, EM is a very slow process and its dynamics is dominated by the smallest magnitude eigenvalues of $\mathbf{A}$. In order to quickly estimate $\mathrm{x}(\tau)$ using (49), we can use the Arnoldi process to reduce the order of the system by capturing these dominant modes. The Arnoldi process produces a smaller Hessenberg matrix of a given size, say m, that approximates the extreme (largest in magnitude) eigenvalues of the original system and an orthonormal basis for projecting the original state vector on to the reduced state vector and vice versa. In our case, we want the reduced order system to approximate the smallest magnitude eigenvalues of $\mathbf{A}$. As such, we apply the Arnoldi process on $\mathbf{A}^{-1}$ because the smallest eigenvalues of $\mathbf{A}$ correspond to the largest eigenvalues of $\mathbf{A}^{-1}$

$$\mathbf{V}_m^T \mathbf{A}^{-1} \mathbf{V}_m = \mathbf{H}_m \tag{50a}$$
$$\mathbf{V}_m^T \mathbf{V}_m = \mathbf{I}_m \tag{50b}$$

where $\mathbf{H}_m \in \mathbb{R}^{m \times m}$ is the Hessenberg matrix, $\mathbf{V}_m \in \mathbb{R}^{q \times m}$ is the orthonormal basis that spans the order-m Krylov subspace of $\mathbf{A}^{-1}$, and $\mathbf{I}_m \in \mathbb{R}^{m \times m}$ is the identity matrix. Using this, we can approximate (49) as [23]

$$\mathrm{x}(\tau) \approx \left\|\hat{\mathrm{x}}(0)\right\|_2 \mathbf{V}_m e^{\tau \mathbf{H}_m^{-1}} e_1 + \mathrm{x}_{ss}. \tag{51}$$

From experiments, we found that $m = 0.05q$ provides a good accuracy versus speed tradeoff. The matrix exponential

in (51) is calculated using the *scaling and squaring method* [23]. In practice, this approximation can be computed quickly because $m \ll q$, and thus can be used to obtain the stress profile of a tree at any given time.

V. Determining Branch Temperatures

Accounting for the temperature distribution across the layers while doing EM analysis is very important due to three reasons. First, the initial residual stress at $t = 0$ for any given tree is mainly due to the thermal stress, which is strongly dependent on the initial temperature [see (9)]. Second, from (4), the diffusivity of branch b_k, which determines the time rate of change of stress, depends on its temperature $T_{m,k}$. Finally, the steady state void length depends on thermal stress: higher thermal stress leads to larger voids. As such, to perform realistic EM checking, one needs to determine the temperature distribution for different layers in the grid. We do this using previous work [24], [25], which we will summarize briefly for completeness.

A. Thermal Modeling

Each layer in the power grid is discretized into uniform volume elements called *thermal blocks* [24]. Each thermal block represents an isothermal volume within a layer, and as such all branches and junctions that reside within a thermal block have the same temperature. For simplicity, we assume that a given branch cannot span two thermal blocks, so that it has no temperature gradient. For each block, we perform thermal analysis using compact thermal modeling (CTM) [25] based on electrothermal equivalence. A CTM is a lumped thermal *RC* network, with heat dissipation modeled as a current source. Specifically, each thermal block is represented as a *thermal node* connected to six resistors, a current source, and a capacitor. The resistors model the heat conductivity to neighboring blocks and their values are determined using thermal properties and geometry of the thermal block

$$g_{\mathrm{E/W}} = 2k_{\mathrm{eff}}\mathrm{b_w b_h}/\mathrm{b_l}, \quad g_{\mathrm{N/S}} = 2k_{\mathrm{eff}}\mathrm{b_l b_h}/\mathrm{b_w}$$
$$g_{\mathrm{up/down}} = 2k_{\mathrm{eff}}\mathrm{b_l b_w}/\mathrm{b_h} \tag{52}$$

where k_{eff} is the effective thermal conductivity and each thermal block has dimension $\mathrm{b_l} \times \mathrm{b_w} \times \mathrm{b_h}$. The total power dissipated in a thermal block can be written as $P = P_{\mathrm{self\_heating}} + P_{\mathrm{logic}}$, where $P_{\mathrm{self\_heating}}$ is due to the average power dissipated by joule heating of the metal branches within the thermal block and P_{logic} is the average heat dissipated by the underlying logic, due to active switching and leakage currents. Note that P_{logic} contributes to power dissipation of thermal nodes in the lowest layer only. In our case, we are only interested in the steady state temperature distribution because transients in temperature occur on a time scale that is small when compared to the EM. Thus, we ignore the thermal capacitance and use the steady state temperature distribution in our analysis.

The number of thermal blocks per layer is the same and is decided based on the required resolution for temperature distribution. In addition, we assume convective boundary condition [24] at the top and insulated boundary conditions at the four sides to model the heat transfer between the power grid and the surroundings. The CTMs for thermal blocks, combined with the boundary conditions, gives us a *thermal grid* that can be solved for finding the temperature distribution of the power grid. We generate the thermal grid at $t = 0$ and calculate the initial temperature distribution to find the residual stress and the branch diffusivities. After a void nucleates, the branch currents change. Hence, we update the $P_{\mathrm{self\_heating}}$ for all thermal nodes, find the new temperature distribution and update the branch diffusivities.

VI. Power Grid EM Analysis

Because EM is a long-term failure mechanism, short-term transients that may be typically experienced in chip workloads do not play a significant role in EM degradation. Hence, and consistent with standard practice in the field, we use an effective-current model [26], so that the grid currents are assumed to be constant at some average (effective) value, at least during the void nucleation phase. Once a void nucleates, branch resistances change fairly quickly and the currents change, also fairly quickly, to new effective values. Thus, between any two successive void nucleations, the grid has fixed currents, voltages, and conductances and so can be modeled using a dc model. To denote the fact that conductances (and the corresponding voltages) change from one nucleation phase to the next, as in [8], we express the grid model as

$$\mathbf{G}(t)v(t) = i_s \tag{53}$$

where $\mathbf{G}(t)$ is the time-varying (but piecewise-constant) conductance matrix, $v(t)$ is the corresponding time-varying (but piecewise constant) vector of node voltage drops, and i_s is the vector of effective values of the current sources tied to the grid.

A. Main Approach

As explained earlier, we use the *mesh model* to find the MTF, in which the grid is deemed to fail not when the first void has nucleated, but when enough voids have nucleated so that the voltage drop specification has exceeded at some grid node. As a byproduct, however, this process also produces the time when the first void nucleates, which helps us generate the MTF under a *series model*, in which a grid is deemed to fail when the first void nucleates. We report the series model MTF for comparison purposes.

We assume that the grid is undamaged (no voids) at $t = 0$. A voltage-drop threshold value for every grid node (or a subset of grid nodes) is given, which is captured in the vector v_{th}. Initially, all node voltage drops are less than v_{th}, i.e., $v(0) < v_{\mathrm{th}}$. A power grid is a collection of interconnect trees. As such, to estimate the EM degradation of the grid, we formulate the LTI system for *every tree* as shown in Section IV-E and numerically integrate it to obtain the stress as a function of position and time. Every time a void nucleates at a junction (i.e., the stress reaches σ_{th}), we pause the integration, calculate the steady state volume of the void and update the branch resistances and current density values. We then check to see if this void leads to an EF, and if it does, we remove the corresponding via from the power grid and update the voltage drops. Then, we determine the new temperature distribution of the grid, update the corresponding boundary conditions and

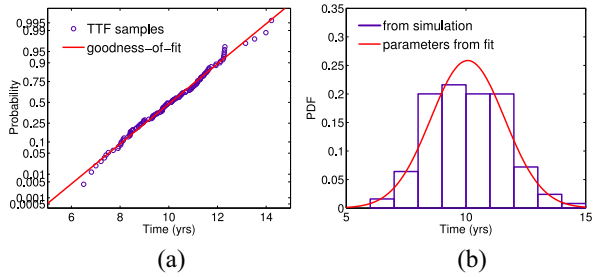

Fig. 6. (a) Goodness-of-fit plot for normal distribution and (b) probability distribution function (pdf) using 125 mesh TTF samples from ibmpg2 *main* approach.

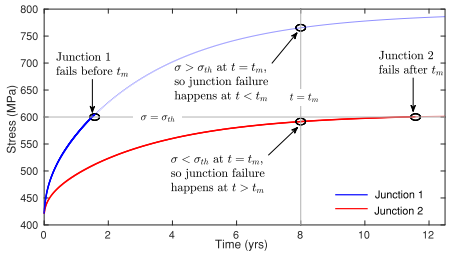

Fig. 7. Idea for filtering scheme. The dotted lines show the *would-be* stress evolution if the boundary conditions are not updated when stress reaches σ_{th}. Junction 1 fails before $t = t_m$, junction 2 fails after.

reformulate the LTI system for all trees using the new boundary conditions. The time of first void nucleation gives the TTF of the grid as per the series model. Due to increase in branch resistances, the voltage drops in the grid continue to increase as we move forward in time. Each time we update the voltage drop, we check to see if a voltage drop violation has occurred somewhere. The earliest time when the voltage drop at any node exceeds v_{th} is the TTF of the grid as per the mesh model.

To account for the random nature of EM degradation, we perform *Monte Carlo random sampling* to estimate the MTF. In each Monte Carlo iteration, we assign new randomly generated diffusivities to all the branches in the grid. This effectively produces a new *instance* of the whole power grid, which we refer to as a *sample grid*. Then, as stated above, we use the LTI system formulation to generate a TTF value based on the series model and another based on the mesh model. With enough samples, we form two averages as our estimates of the series MTF and the mesh MTF.

Let $\mathbf{T}$ be the RV that represents the statistics of the mesh TTF for this approach, then the expected value of $\mathbf{T}$, denoted by $E[\mathbf{T}]$, is the mesh MTF of the grid. Using goodness of fit methods, it was found that the normal distribution is a good fit for $\mathbf{T}$ (see Fig. 6). Therefore, we can use standard statistical sampling (Monte Carlo) [27] to find the value of $E[\mathbf{T}]$ to within a user-specified error tolerance. The number of samples required for Monte Carlo to terminate is determined such that we have $(1-\lambda)\times 100\%$ confidence (e.g., $\lambda = 0.05$ for 95% confidence) that the relative error in MTF estimation is less than a user-provided relative error threshold ϵ (e.g., $\epsilon = 0.1$ for 10% relative error threshold).

Though this is the most accurate approach, numerically solving *all* the trees in the power grid using the extended Korhonen's model can be computationally expensive. In this paper, we use this approach only on smaller grids and we refer to it as the *main approach*. The results from this approach serve as a benchmark of comparison for more optimized approaches.

B. Improved Performance With Filtering

We will now present a method that drastically reduces the run-time with almost no impact on accuracy. We will refer this as the *Filtering* approach. For each *sample grid*, solving all the trees up to the time of grid failure yields a specific sequence of void nucleation times in certain trees that are of interest. In particular, all trees that nucleate their first void *before* the time of grid failure are of interest to us. All trees that nucleate their first void *after* the grid failure are inconsequential to us, and we would do well to not solve them in the first place. Unfortunately, we do not know up-front which set of trees should be solved, and which can be discarded. However, we can devise an approximate filtering scheme that indicates which subset of trees will most likely nucleate before all the rest. We call this subset as the *active set*.

For a given sample grid, we restrict our attention to trees whose estimated first void nucleation times are *smaller* than some threshold $t = t_m$. Note that we do not need to know the exact time of void nucleation(s) for junctions in a tree, rather we only need to know if the first void nucleates before t_m. Clearly, if the stress evolution at a junction is to cause void nucleation before time t_m, then that junction's *would-be* stress value at t_m is higher than σ_{th} (see Fig. 7). Here, the *would-be* stress value at t_m denotes the hypothetical stress value at a junction if the boundary conditions are not updated at the time of void nucleation. We use the macromodeling-based solution (51) to calculate the *would-be* stress profile of every tree at $t = t_m$, and any tree with junction stresses greater than σ_{th} at $t = t_m$ is included in the active set. We refer to t_m as the *active set cutoff threshold* and it is a part of the Monte Carlo process. We start with a sufficiently high value for t_m, that is reduced as more TTF samples are obtained.

Trees that are likely to nucleate before t_m, based on this filtering scheme, are declared to be part of the active set and are numerically solved. If the *sample grid* fails before t_m, we obtain a sample TTF. On the other hand, it might be the case that the sample grid has not failed up to $t = t_m$. In this case, we set the TTF sample equal to t_m, and such a sample is called a *limited sample*. Thus, in our Monte Carlo approach, we effectively sample from the RV $\mathbf{T}'$ that has a *limited normal distribution* ($l = -\infty$ and $u = t_m$) with the underlying normal RV $\mathbf{T}$. However, we can estimate the mean of the underlying RV $E[\mathbf{T}]$ using the samples obtained from the limited RV $\mathbf{T}'$, as shown next.

Using the *law of total expectation* [28], we can write for $\mathbf{T}$

$$E[\mathbf{T}] = E[\mathbf{T}|\mathbf{T} \le t_m]F(t_m) + E[\mathbf{T}|\mathbf{T} > t_m](1 - F(t_m)) \qquad (54)$$

where $F(t)$ is the cdf of the normal RV $\mathbf{T}$. We can also express $E[\mathbf{T}']$ in similar terms. From the definition of a limited RV, we have $E[\mathbf{T}'|\mathbf{T}' \le t_m] = E[\mathbf{T}|\mathbf{T} \le t_m]$, $E[\mathbf{T}'|\mathbf{T}' > t_m] = t_m$, and $F'(t_m) = F(t_m)$, with $F'(t)$ being the cdf of RV $\mathbf{T}'$.

Hence, we can write

$$E[\mathbf{T}'] = E[\mathbf{T}|\mathbf{T} \le t_m]F(t_m) + t_m(1 - F(t_m)). \quad (55)$$

Subtracting (55) from (54), we get

$$\begin{aligned} E[\mathbf{T}] &= E[\mathbf{T}'] + (E[\mathbf{T}|\mathbf{T} > t_m] - t_m)(1 - F(t_m)) \\ &= E[\mathbf{T}'] + E[\mathbf{T} - t_m|\mathbf{T} > t_m](1 - F(t_m)). \end{aligned} \quad (56)$$

The term $E[\mathbf{T} - t_m|\mathbf{T} > t_m]$ is the mean residual life (MRL) of the power grid at $t = t_m$. Define $\mu \triangleq E[\mathbf{T}]$, $\mu' \triangleq E[\mathbf{T}']$, and $p_f \triangleq F(t_m)$. Since we know that $\mathbf{T}$ has a normal distribution, the MRL of the power grid at $t = t_m$ can be expressed in terms of μ and p_f. From (56), after some algebraic manipulation, we obtain

$$\mu = \frac{\mu' + (\kappa - 1)t_m}{\kappa} \quad (57)$$

where $\kappa = p_f + \phi(\Phi^{-1}(p_f))/\Phi^{-1}(p_f)$, $\Phi(t)$ and $\phi(t)$ are, respectively, the cdf and pdf of a standard normal distribution $\mathcal{N}(0, 1)$. Φ^{-1} denotes the inverse cdf of $\mathcal{N}(0, 1)$ which can be computed on most operating systems using the `erfinv()` function. We estimate μ' and p_f from the statistical sampling process. Let $\{T'_1, T'_2, \ldots T'_s\}$ be s samples obtained from RV $\mathbf{T}'$ using a Monte Carlo process. Then, define

$$\hat{\mu}' \triangleq \frac{1}{s}\sum_{k=1}^{s} T'_k, \quad \hat{p}_f \triangleq 1 - \frac{\left|\{T'_k : T'_k > t_m\}\right|}{s} \quad (58)$$

where $\hat{\mu}'$ is the *estimated* value of μ' and $\hat{p}_f$ is the *estimated* value of p_f. Thus, using $\hat{\mu}'$ and $\hat{p}_f$ in (57) we can calculate $\hat{\mu}$, the estimated value of μ. Note that μ', p_f, and μ are the *true* values, so that $\lim_{s\to\infty}\hat{\mu}' = \mu'$, $\lim_{s\to\infty}\hat{p}_f = p_f$, and $\lim_{s\to\infty}\hat{\mu} = \mu$. Then, the error in estimation can be written as: $\delta\mu = |\hat{\mu} - \mu|$, $\delta\mu' = |\hat{\mu}' - \mu'|$, and $\delta p_f = |\hat{p}_f - p_f|$.

Similar to the *main* approach, we stop the Monte Carlo process when we are $(1-\lambda)\times 100\%$ confident that the relative error in estimated MTF is less than some user provided threshold ϵ. In other words, we stop if

$$\frac{\delta\mu_\lambda}{\mu} \le \epsilon \iff \frac{\delta\mu_\lambda}{\hat{\mu}} \le \frac{\epsilon}{1+\epsilon} \quad (59)$$

where $\delta\mu_\lambda$ is $(1-\lambda) \times 100\%$ confidence bound on the estimation error $\delta\mu$. In other words, this means that the interval $[\hat{\mu} - \delta\mu_\lambda, \hat{\mu} + \delta\mu_\lambda]$ will contain μ (the true value) $(1 - \lambda) \times 100\%$ of the time. Using propagation of errors [29] in (57), we get

$$\delta\mu_\lambda = \sqrt{\left(\frac{\partial\mu}{\partial\mu'}\delta\mu'_\lambda\right)^2 + \left(\frac{\partial\mu}{\partial p_f}\delta p_{f\lambda}\right)^2} \quad (60)$$

where $\delta\mu'_\lambda$ and $\delta p_{f\lambda}$ are the $(1-\lambda)\times 100\%$ confidence bounds on μ' and p_f, respectively. $\delta\mu'_\lambda$ is obtained from simulation, using the technique given in [21] and $\delta p_{f\lambda}$ can be calculated from the TTF samples using [30]. For lack of space, we skip the details and present the final expression

$$\begin{aligned} \delta\mu_\lambda^2 = &\frac{(\delta\mu'_\lambda)^2}{\hat{\kappa}^2} \\ &+ \frac{z^2_{\lambda/2}(t_m - \hat{\mu}')^2\hat{p}_f(1-\hat{p}_f)}{\hat{\kappa}^4 s}\left[1 + \left(1 + \frac{1}{y^2}\right)^2\right] \end{aligned} \quad (61)$$

TABLE I
COMPARISON OF POWER GRID MTF USING THE MAIN APPROACH AND FILTERING APPROACH

Grid Name	Main			Filtering			Error (%)		Speed Up
	$\mu_s^{\mathtt{all}}$ (yrs)	$\mu_m^{\mathtt{all}}$ (yrs)	time (hrs)	$\mu_s^{\mathtt{act}}$ (yrs)	$\mu_m^{\mathtt{act}}$ (yrs)	time (hrs)	Series	Mesh	
ibmpg1	4.38	10.98	0.13	4.52	10.69	0.11	3.14	2.61	1.23x
ibmpg2	6.49	9.79	1.46	6.50	9.72	0.39	0.25	0.74	3.72x
ibmpg5	4.56	6.21	15.6	4.56	6.18	0.26	0.10	0.46	59.98x

where $z_{\lambda/2}$ is the $(1 - \lambda/2)$-percentile of $\mathcal{N}(0, 1)$, $\hat{\kappa} = \hat{p}_f + \phi(y)/y$ and $y = \Phi^{-1}(\hat{p}_f)$. We obtain at least 30 TTF samples before starting to check the stopping criteria (59).

C. TTF Predictor Approach

We next describe a predictor-based approach to further speed up the MTF computation. This approach is applied on top of the filtering approach explained earlier and gives excellent speed-ups. It makes use of the reduced-order model given in Section IV-F earlier.

Once the stress profile of a tree is determined for a few time-points using (51), it should be possible to extrapolate the rest of the trend, with some suitably nonlinear fitting function. The fitting function can thus be used as a *TTF predictor*, to find a good estimate of the nucleation times for all junctions within the tree. Parameters of the function can be found using least-squares fitting, based on the points already solved. While various exponential or log functions may be suitable, we have found empirically that the following power function template provides a very good fit:

$$f(t) = at^{b + c\ln t} \quad (62)$$

where a, b, and c are parameters to be determined using regression analysis and least-squares fitting and $f(t)$ is the stress value at time t. Note that $\ln(f(t))$ is a simple quadratic in $\ln t$, with $\ln a$, b, and c as the three coefficients. Once we estimate the time of void nucleations using (51) and the TTF predictor, we can predict the time (and sequence) of void nucleations. For each void nucleation, we update the corresponding branch resistances and voltage drops until the grid fails.

VII. EXPERIMENTAL RESULTS

All approaches have been implemented in `C++` and tested on a number of IBM power grid benchmarks [16], using a quad-core 3.4 GHz Linux machine with 32GB of RAM. The interconnect material is assumed to be copper, so that the following parameters are used in our EM model: $B = 1.35 \times 10^{11}$ Pa, $\Omega = 1.66 \times 10^{-29}$ m^3, $k_b = 1.38 \times 10^{-23}$ J/K, $q^* = 8.0109 \times 10^{-19}$ C, $\sigma_{\text{th}} = 600 \times 10^6$ Pa [9], and $\delta = 10^{-9}$ m. An ambient temperature of 300 K is used for all simulations. Each branch is discretized into $N = 16$ segments. We use a relative tolerance of 10^{-3} and an absolute tolerance of 10^{-6} for the ODE solver. For all grids, we used $\lambda = 0.05$ (95% confidence bounds) and $\epsilon = 0.1$ (maximum relative error threshold of 10%). In our implementation, we use a *shared memory model* to parallelize the computation.

Table I compares the accuracy and runtime of the *main* approach versus the *filtering* approach. Since the *main*

TABLE II
COMPARISON OF POWER GRID MTF AS ESTIMATED USING BLACK'S MODEL AND EXTENDED KORHONEN'S MODEL

Power Grid				Black's Model			Extended Korhonen's Model							
							Filtering			Filtering + Predictor				
Grid Name	# nodes	#branches	#trees	$\mu_s^{\mathtt{blk}}$ (yrs)	$\mu_m^{\mathtt{blk}}$ (yrs)	$t_{\mathtt{blk}}$ (hrs)[a]	$\mu_s^{\mathtt{act}}$ (yrs)	$\mu_m^{\mathtt{act}}$ (yrs)	$t_{\mathtt{act}}$ (hrs)[a]	$\mu_s^{\mathtt{pre}}$ (yrs)	$\mu_m^{\mathtt{pre}}$ (yrs)	$t_{\mathtt{pre}}$ (hrs)[a]	$\frac{\mu_m^{\mathtt{act}}}{\mu_m^{\mathtt{blk}}}$	$\frac{t_{\mathtt{act}}}{t_{\mathtt{pre}}}$
ibmpg1	6K	11K	709	5.39	9.13	0.001	4.52	10.69	0.11	4.19	10.90	0.003	1.17	33.59x
ibmpg2	62K	61K	462	2.96	6.33	0.03	6.50	9.72	0.39	6.53	10.11	0.04	1.54	9.86x
ibmpg3	410K	401K	8.1K	2.92	6.62	0.26	4.11	10.04	10.79	4.12	9.95	0.41	1.52	26.61x
ibmpg4	475K	465K	9.6K	1.38	2.97	0.53	4.95	9.45	9.25	4.96	11.95	2.31	3.18	4.01x
ibmpg5	249K	496K	2K	2.26	3.61	0.02	4.56	6.18	0.26	4.50	6.63	0.06	1.71	4.21x
ibmpg6	404K	798K	10.2K	1.20	1.32	0.02	4.79	10.11	4.40	4.84	11.96	0.79	7.67	5.59x
ibmpgnew1	316K	698K	19.5K	1.18	2.64	0.14	2.39	10.36	1.72	2.32	11.64	1.24	3.92	1.39x
ibmpgnew2	718K	698K	19.5K	1.62	4.82	0.68	3.44	6.18	1.22	3.48	6.72	0.43	1.28	2.87x

[a] $t_{\mathtt{blk}}$, $t_{\mathtt{act}}$ and $t_{\mathtt{pre}}$ denote the run-time(s) for Black's model, Filtering and predictor based approaches, respectively.

approach slows down considerably as the grid size increases, we were able to test it only on the three smallest benchmarks. $\mu_m^{\mathtt{all}}$ ($\mu_s^{\mathtt{all}}$) and $\mu_m^{\mathtt{act}}$ ($\mu_s^{\mathtt{act}}$) denote the estimated mesh (series) MTF using the main approach and the filtering approach, respectively. From Table I, it is clear that as the grid size increases, the filtering approach leads to significant speed-ups with negligible loss in accuracy. For the largest grid we could test (ibmpg5 with 2002 trees), the filtering approach obtained a speed-up of $\sim$ **60**$\times$ over the *main* approach with error in series MTF estimation being only 0.1% and the error in mesh MTF being 0.46%. This shows the value of the filtering approach.

Table II lists the MTFs estimated per the series and mesh models using three approaches, based on: 1) Black's model (columns $\mu_s^{\mathtt{blk}}$ and $\mu_m^{\mathtt{blk}}$) implemented to give a mesh MTF as in [8]; 2) our extended Korhonen's model with the active set filter ($\mu_s^{\mathtt{act}}$ and $\mu_m^{\mathtt{act}}$); and 3) our extended Korhonen's model with the active set filter and the TTF predictor ($\mu_s^{\mathtt{pre}}$ and $\mu_m^{\mathtt{pre}}$). In order to give a fair comparison, we calibrate Black's model based on data obtained from Korhonen's model. From the table, we note that $\mu_s^{\mathtt{act}} > \mu_s^{\mathtt{blk}}$ and $\mu_m^{\mathtt{act}} > \mu_m^{\mathtt{blk}}$ for all grids, except ibmpg1 for which the estimated series MTF using Black's model is longer than that estimated using our approach. Overall, the mesh (series) MTF estimated using the extended Korhonen's model is 2.75$\times$ (2.27$\times$) longer than that found using Black's model. Finally, in Table II we also report the MTF values obtained using the TTF predictor approach. As compared to the filter-only approach, the predictor-based variation achieves an average speed-up of $\sim$**11**$\times$ for all reported grids, with average error in the mesh (series) MTF being 10% (1.8%).

In order to show the inaccuracy in Black's model, we present two scenarios, based on two interconnect trees $\mathcal{T}_1$ and $\mathcal{T}_2$ taken from ibmpg2. Both trees are straight metal stripes with 192 branches each. $\mathcal{T}_1$ has a high current density profile, with maximum branch current density being 5.31×10^9 A/m^2 [Fig. 8(a)]. In this case, Black's model predicts the first failure time of about 6.2 years, whereas the actual failure time found using the extended Korhonen's model is around 13.2 years, which is $\sim$2$\times$ longer. $\mathcal{T}_2$ has a low current density profile, with maximum branch current density being 1.44×10^9 A/m^2 [Fig. 9(a)]. Here, due to the Blech effect, Black's model predicts that no failure would occur. However, accounting for the material flow between the branches and temperature gradients, we found that the first failure would occur around 2.44 years. Thus, Black's model was pessimistic in the first scenario and highly optimistic in the second one. This shows that lifetime estimates using the Black's model can be highly inaccurate.

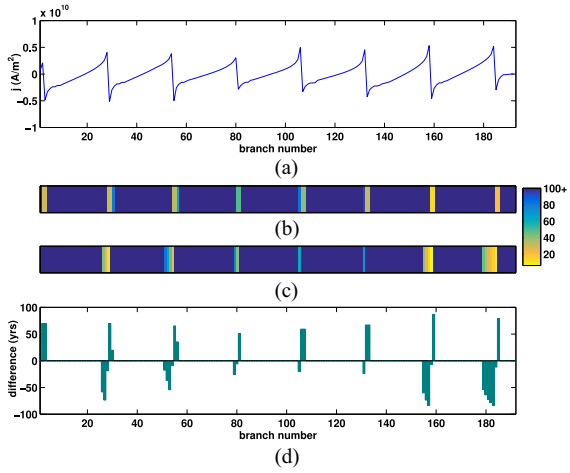

Fig. 8. (a) Current density profile for $\mathcal{T}_1$ and MTFs estimated using (b) extended Korhonen's model ($\mathrm{MTF}_{\mathrm{ekm}}$), (c) Black's model ($\mathrm{MTF}_{\mathrm{blk}}$), and (d) $\mathrm{MTF}_{\mathrm{blk}} - \mathrm{MTF}_{\mathrm{ekm}}$.

We also explore the effect of temperature on the lifetimes estimated using the extended Korhonen's model. For this comparison, we use $\mathcal{T}_1$. We first estimate the MTFs using the actual temperature distribution, as shown in Fig. 11(a). For this case, the first failure happens around 13.2 years. Now, we artificially assume a constant temperature of 325 K throughout the tree. Note that 325 K is the average of the actual branch temperatures. In this case, the first failure happens around 20.26 years. A higher nominal temperature would result in a lower failure time and vice versa. Hence, temperature distribution plays a very important role and should be taken into account while doing EM analysis.

In order to assess the impact of EFs on the grid lifetime, we present a case study using the ibmpg2 grid; we estimate its mesh MTF under two settings, one where EF detection is on and the other where EF detection is turned off. As

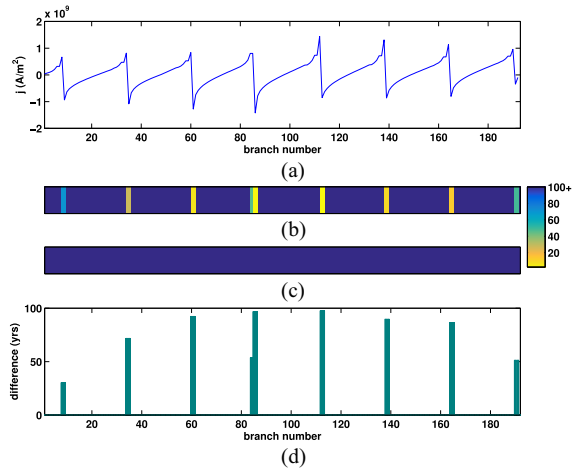

Fig. 9. (a) Current density profile for $\mathcal{T}_2$ and MTFs estimated using (b) extended Korhonen's model (MTF_{ekm}), (c) Black's model (MTF_{blk}), and (d) $\text{MTF}_{\text{blk}} - \text{MTF}_{\text{ekm}}$.

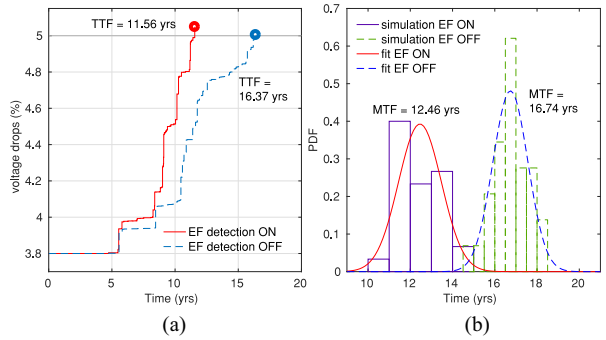

Fig. 10. Impact of EF on (a) voltage drops (shown for one sample grid) and (b) estimated mesh MTF for ibmpg2. Maximum voltage drop at $t = 0$ is $3.8\%v_{dd}$, and $v_{\text{th}} = 5\%v_{dd}$.

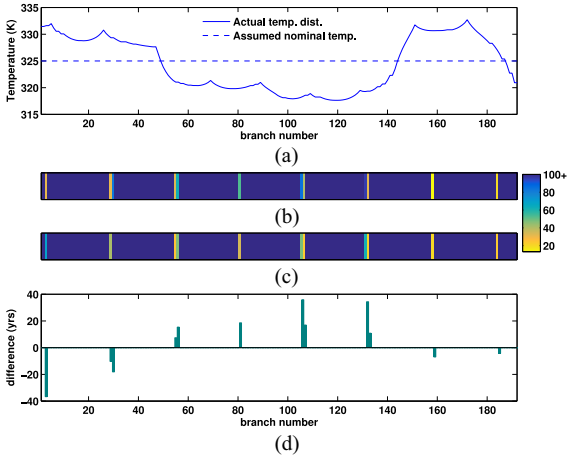

Fig. 11. (a) Actual temperature profile and the assumed nominal temperature distribution. MTFs estimated with (b) actual temperature profile (MTF_T), (c) assuming $T_m = 325\text{K}$ for all branches ($\overline{\text{MTF}_T}$), and (d) $\text{MTF}_T - \overline{\text{MTF}_T}$.

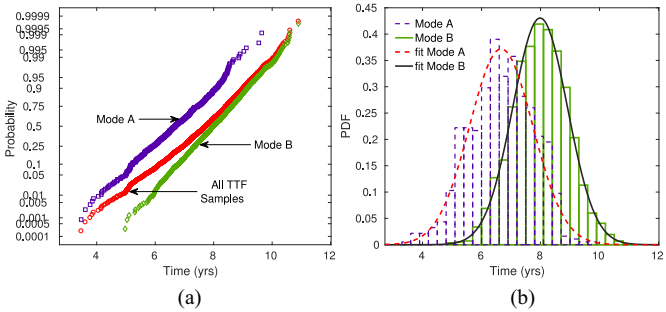

Fig. 12. (a) Probability plot and (b) empirical pdf obtained using 2500 mesh TTF samples of ibmpg2 grid shows an underlying bimodal distribution for different modes of grid failure. $\text{MTF}_A = 6.67$ yrs, $\text{MTF}_B = 7.99$ yrs, $\text{MTF}_{\text{all}} = 7.66$ yrs.

can be seen from Fig. 10(b), turning off EFs gives an optimistic MTF estimate which is 34% longer than the actual MTF. Thus, if the target product lifetime is set as 15 years, this grid will fail EM sign off due to the impact of EFs, but would erroneously succeed if EFs are ignored. The difference in MTFs stems from the influence of EFs on node voltage drops. In Fig. 10(a), we show how the maximum node voltage drop changes with time as voids nucleate due to EM. Since EFs lead to an open circuit, their impact on voltage drops is more severe, which leads to shorter lifetimes. In general, the effect of EFs gets more pronounced as the difference between the maximum initial voltage drop and v_{th} increases.

Statistical analysis of EM failures in copper interconnects often shows bimodal distributions due to the presence of EFs [31]. A similar bimodal distribution can be observed in the statistics for mesh TTF samples obtained using our power grid EM analysis. Consider the following two failure modes for a given *sample grid: Mode A*, in which all junction failures that lead to grid failure are EFs and *Mode B*, where at least one junction failure is a conventional failure. Fig. 12(a) and (b) show, respectively, the probability plot the empirical pdf for the two failure modes obtained using 2500 mesh TTF samples from ibmpg2. Since the pdf for failure modes A and B have a lot of overlap, the overall distribution is almost normal.

VIII. Conclusion

We proposed a physics-based EM checking approach for on-die power grids that removes the unrealistic assumptions inherent in traditional industrial tools. Our approach accounts for process and cross die temperature variations and detects EFs. Computational speed is improved using a macromodeling-based filtering scheme and a fast predictor-based approach, with minimal impact on accuracy. The MTFs estimated using our physics-based approach were $2.75\times$ longer on average than those based on a (calibrated) Black's model. The method is quite fast and is suitable for very large power grids.

References

[1] J. Warnock, "Circuit design challenges at the 14nm technology node," in *Proc. 48th ACM/EDAC/IEEE Design Autom. Conf. (DAC)*, New York, NY, USA, Jun. 2011, pp. 464–467.

[2] A. S. Oates, "Interconnect reliability challenges for technology scaling: A circuit focus," in *Proc. IEEE Int. Interconnect Technol. Conf. Adv. Metallization Conf. (IITC/AMC)*, San Jose, CA, USA, May 2016, p. 59.

[3] J. R. Black, "Electromigration—A brief survey and some recent results," *IEEE Trans. Electron Devices*, vol. 16, no. 4, pp. 338–347, Apr. 1969.

[4] M. Hauschildt *et al.*, "Electromigration early failure void nucleation and growth phenomena in Cu and Cu(Mn) interconnects," in *Proc. IEEE Int. Rel. Phys. Symp. (IRPS)*, Anaheim, CA, USA, Apr. 2013, pp. 2C.1.1–2C.1.6.
[5] J. Lloyd, "Black's law revisited—Nucleation and growth in electromigration failure," *Microelectron. Rel.*, vol. 47, nos. 9–11, pp. 1468–1472, 2007.
[6] I. A. Blech, "Electromigration in thin aluminum films on titanium nitride," *J. Appl. Phys.*, vol. 47, no. 4, pp. 1203–1208, 1976.
[7] C. L. Gan, C. V. Thompson, K. L. Pey, and W. K. Choi, "Experimental characterization and modeling of the reliability of three-terminal dual-damascene Cu interconnect trees," *J. Appl. Phys.*, vol. 94, no. 2, pp. 1222–1228, 2003.
[8] S. Chatterjee, M. Fawaz, and F. N. Najm, "Redundancy-aware electromigration checking for mesh power grids," in *Proc. IEEE/ACM Int. Conf. Comput.-Aided Design*, San Jose, CA, USA, Nov. 2013, pp. 540–547.
[9] X. Huang, Y. Tan, V. Sukharev, and S. X.-D. Tan, "Physics-based electromigration assessment for power grid networks," in *Proc. ACM/EDAC/IEEE Design Autom. Conf.*, San Francisco, CA, USA, Jun. 2014, pp. 1–6.
[10] M. A. Korhonen, P. Borgesen, K. N. Tu, and C.-Y. Li, "Stress evolution due to electromigration in confined metal lines," *J. Appl. Phys.*, vol. 73, no. 8, pp. 3790–3799, 1993.
[11] S. P. Hau-Riege and C. V. Thompson, "Experimental characterization and modeling of the reliability of interconnect trees," *J. Appl. Phys.*, vol. 89, no. 1, pp. 601–609, 2001.
[12] D.-A. Li, M. Marek-Sadowska, and S. R. Nassif, "A method for improving power grid resilience to electromigration-caused via failures," *IEEE Trans. Very Large Scale Integr. (VLSI) Syst.*, vol. 23, no. 1, pp. 118–130, Jan. 2015.
[13] X. Huang *et al.*, "Electromigration assessment for power grid networks considering temperature and thermal stress effects," *Integr. VLSI J.*, vol. 55, pp. 307–315, Sep. 2016.
[14] D.-A. Li, M. Marek-Sadowska, and S. R. Nassif, "T-VEMA: A temperature-and variation-aware electromigration power grid analysis tool," *IEEE Trans. Very Large Scale Integr. (VLSI) Syst.*, vol. 23, no. 10, pp. 2327–2331, Oct. 2015.
[15] S. Chatterjee, V. Sukharev, and F. N. Najm, "Fast physics-based electromigration checking for on-die power grids," in *Proc. 35th Int. Conf. Comput.-Aided Design*, Austin, TX, USA, Nov. 2016, pp. 1–8.
[16] S. R. Nassif, "Power grid analysis benchmarks," in *Proc. ASP-DAC*, Seoul, South Korea, 2008, pp. 376–381.
[17] B. Li, J. Gill, C. J. Christiansen, T. D. Sullivan, and P. S. McLaughlin, "Impact of via-line contact on Cu interconnect electromigration performance," in *Proc. IEEE Int. Rel. Phys. Symp.*, San Jose, CA, USA, Apr. 2005, pp. 24–30.
[18] J. J. Clement, "Electromigration modeling for integrated circuit interconnect reliability analysis," *IEEE Trans. Device Mater. Rel.*, vol. 1, no. 1, pp. 33–42, Mar. 2001.
[19] J. R. Lloyd and J. Kitchin, "The electromigration failure distribution: The fine-line case," *J. Appl. Phys.*, vol. 69, no. 4, pp. 2117–2127, Feb. 1991.
[20] W. Schiesser, *Computational Mathematics in Engineering and Applied Science: ODEs, DAEs, and PDEs*. Boca Raton, FL, USA: CRC Press, 1994.
[21] I. Bebu and T. Mathew, "Confidence intervals for limited moments and truncated moments in normal and lognormal models," *Stat. Probab. Lett.*, vol. 79, no. 3, pp. 375–380, 2009.
[22] V. Sukharev, A. Kteyan, and X. Huang, "Postvoiding stress evolution in confined metal lines," *IEEE Trans. Device Mater. Rel.*, vol. 16, no. 1, pp. 50–60, Mar. 2016.
[23] N. J. Highham, *Functions of Matrices: Theory and Computation*. Philadelphia, PA, USA: Soc. Ind. Appl. Math., 2008.
[24] Y.-K. Cheng, P. Raha, C.-C. Teng, E. Rosenbaum, and S.-M. Kang, "ILLIADS-T: An electrothermal timing simulator for temperature-sensitive reliability diagnosis of CMOS VLSI chips," *IEEE Trans. Comput.-Aided Design Integr. Circuits Syst.*, vol. 17, no. 8, pp. 668–681, Aug. 1998.
[25] W. Huang *et al.*, "HotSpot: A compact thermal modeling methodology for early-stage VLSI design," *IEEE Trans. Very Large Scale Integr. (VLSI) Syst.*, vol. 14, no. 5, pp. 501–513, May 2006.
[26] L. M. Ting, J. S. May, W. R. Hunter, and J. M. McPherson, "AC electromigration characterization and modeling of multilayered interconnects," in *Proc. IEEE Int. Rel. Phys. Symp.*, Atlanta, GA, USA, Mar. 1993, pp. 311–316.
[27] I. Miller, J. E. Freund, and R. Johnson, *Probability and Statistics for Engineers*. Englewood Cliffs, NJ, USA: Prentice-Hall, Inc, 1990.
[28] N. A. Weiss, P. T. Holmes, and M. Hardy, *A Course in Probability*. Boston, MA, USA: Pearson, 2005.
[29] H. H. Ku, "Notes on the use of propagation of error formulas," *J. Res. Nat. Bureau Stand. C Eng. Instrum.*, vol. 70C, no. 4, pp. 263–273, 1966.
[30] L. D. Brown, T. T. Cai, and A. DasGupta, "Interval estimation for a binomial proportion," *Stat. Sci.*, vol. 16, no. 2, pp. 101–117, 2001.
[31] E. T. Ogawa *et al.*, "Statistics of electromigration early failures in Cu/oxide dual-damascene interconnects," in *Proc. 39th Annu. IEEE Int. Rel. Phys. Symp.*, Orlando, FL, USA, 2001, pp. 341–349.

Sandeep Chatterjee (S'14) received the B.Tech. (with high Distinction) degree in electrical engineering from the Indian Institute of Technology Roorkee, Roorkee, India, in 2011, and the M.A.Sc. degree in electrical and computer engineering from the University of Toronto, Toronto, ON, Canada, in 2013, where he is currently pursuing the Ph.D. degree with the Department of Electrical and Computer Engineering.

His current research interests include computer-aided design for integrated circuits with a focus on the reliability, verification, and analysis of power grids.

Mr. Chatterjee was a recipient of the Best Paper Award from the International Conference on Computer-Aided Design.

Valeriy Sukharev received the Ph.D. degree in physical chemistry from the Russian Academy of Sciences, Moscow, Russia.

He is a Technical Lead with the Design to Silicon Division (Calibre), Mentor Graphics Corporation, Fremont, CA, USA. His current research interests include development of new full-chip modeling and simulation capabilities for the electronic design automation, semiconductor processing, and reliability management.

Dr. Sukharev was a recipient of the 2014 Mahboob Khan Outstanding Industry Liaison/Associate Award. He serves on the editorial boards and technical/steering committees of a number of profiling journals and conferences.

Farid N. Najm (S'85–M'89–SM'96–F'03) received the B.E. degree in electrical engineering from the American University of Beirut, Beirut, Lebanon, in 1983, and the Ph.D. degree in electrical and computer engineering (ECE) from the University of Illinois at Urbana–Champaign (UIUC), Champaign, IL, USA, in 1989.

He is a Professor with the Edward S. Rogers Sr. Department of ECE, University of Toronto, Toronto, ON, Canada. From 1989 to 1992, he was with Texas Instruments, Dallas, TX, USA. He then joined the ECE Department with UIUC as an Assistant Professor and became an Associate Professor in 1997. In 1999, he joined the ECE Department with the University of Toronto, where he is currently a Professor and the Chair. He has authored the book entitled *Circuit Simulation* (Wiley, New York, NY, USA, 2010). His current research interests include CAD for very large scale integration, with an emphasis on circuit level issues related to power, timing, variability, and reliability.

Dr. Najm was a recipient of the IEEE TRANSACTIONS ON COMPUTER-AIDED DESIGN OF INTEGRATED CIRCUITS AND SYSTEMS Best Paper Award, the NSF Research Initiation Award, the NSF CAREER Award, the Design Automation Conference Prolific Author Award, and the Best Paper Award from the International Conference on Computer-Aided Design. He was an Associate Editor of the IEEE TRANSACTIONS ON VERY LARGE SCALE INTEGRATION (VLSI) SYSTEMS from 1997 to 2002, and the IEEE TRANSACTIONS ON COMPUTER-AIDED DESIGN OF INTEGRATED CIRCUITS AND SYSTEMS from 2001 to 2009. He served on the executive committee for the International Symposium on Low-Power Electronics and Design (ISLPED) from 1999 to 2013 and has served as the TPC Chair and the General Chair for ISLPED. He is a fellow of the Canadian Academy of Engineering.